Renewable Energy 190 (2022) 560–571

Contents lists available at ScienceDirect

Renewable Energy

journal homepage: www.elsevier.com/locate/renene

Assessing low frequency variations in solar and wind power and their climatic teleconnections

Emilio Bianchi*, Tomás Guozden, Roberto Kozulj

Universidad Nacional de Río Negro, Argentina

ARTICLE INFO

Article history:
Received 15 August 2021
Received in revised form
23 February 2022
Accepted 13 March 2022
Available online 31 March 2022

Keywords:
Solar power
Wind power
Climate variability
Extreme events

ABSTRACT

Power grids are being increasingly exposed to climatic variability due to the addition of renewables, but low frequency climate variations are often poorly captured in the measuring campaigns. We analyzed the co-occurrence of low frequency variations in the wind and solar resources over Argentina, and discuss climatic mechanisms behind those variations. We found low complementarity between periods of high and low availability of wind and solar resources. We found a negative relationship between the wind resource and the Antarctic Oscillation. Regarding the solar resource, we found a negative relationship with an index of the El Niño phenomenon; we also found positive relationships with two oceanic indices of the Atlantic variability. The relationships with these Atlantic drivers seem to be associated to low frequency variations, while El Niño relates to inter annual variations. Composites of oceanic and atmospheric anomalies reveal that changes in cloudiness respond to variations in the flux of water vapor over South America which, in turn, seem to be part of the atmospheric features of El Niño; and are also coherent with previous studies linking precipitation variations over subtropical South America and Sea Surface Temperatures over the Atlantic.

1. Introduction

Electrical grids around the world are being increasingly exposed to climatic and synoptic variability due to the rapid addition of climate-dependent renewable capacity [1–3]. Until recently, the impact of meteorological variations on these systems was restricted to the relationship between weather and electricity consumption (mainly due to cooling and heating) [4–6], and the availability of water for hydro generation [7,8]. Nowadays, climate-dependent renewables (mainly wind and solar) are reaching significant shares in the electricity generation mixes in several countries [9], which imposes significant challenges in the operation and planning of electricity grids [10,11].

Wind speeds and solar radiation vary on multiple timescales: From seconds to minutes (associated with turbulent eddies and the passage of clouds), the diurnal cycle, synoptic scale variations associated to weather systems, an annual cycle, and interannual variations which are associated to long term trends and/or low frequency variations [12–14]. The impacts of these variations on power systems are different according to the timescale considered [15]. High frequency variations have implications in the operational aspects (frequency control, load following, unit commitment), while low frequency variations are important when considering long term planning and design, and resource assessment [16]. As an example, seasonal predictions of wind speeds, as reported in Ref. [17], can help in the estimation of use of other resources.

Low frequency variations are receiving increasing attention [6,13,18,19]. These low frequency variations are poorly captured in the measuring campaigns of individual wind and solar facilities, even though they might condition their economical flows and risks [20–22]. Furthermore, from the perspective of grid operators and planners, low frequency variability is an important factor when planning fuel or hydro reserves and in the long term design of the system [13].

Low frequency variability can be characterized by the use of long-term climate data [23,24]. The estimation of the frequency of occurrence of rare or extreme climatological events can be performed by the establishment of some kind of threshold on the variable being studied [25,26]. This enables the identification of the onset, duration, end, severity and spatial extent of any extreme event, and allows to describe it statistically [27–29]. This procedure is widely applied in hydrology [25,30,31]. Drought indices are

* Corresponding author.
E-mail address: ebianchi@unrn.edu.ar (E. Bianchi).

https://doi.org/10.1016/j.renene.2022.03.080
0960-1481/

important inputs for an accurate water management policy and declaration and mitigation of extreme hydrological events [29,32]. Other users could make use of these tools by applying similar analyses on other climate variables [33]. Nevertheless, this is not a common practice in energy meteorology studies with some exceptions such as Malloy et al. (2015) [33] and Dawkins and Rushby [26]. [33] provide a thorough climatological assessment of surface *wind lulls* [34] and *wind blows*, defined as mean monthly wind speeds *1* standard deviation below and above the long-term mean annual at each grid point over a large domain covering north America; and [26] implements a 90th percent threshold on a residual demand index to define periods of adverse weather. Besides a statistical description, other authors suggest that it is also necessary to gain insight into the synoptic and climatic drivers associated with such events [35,36].

Climate variability is often associated with a limited number of known climatic drivers [37], which might be rooted on the tropical oceans [38] or reflect mid and high latitude atmospheric circulation shifts [39]; and whose areas of influence range from regional to global [40]. For these reason, studies addressing low-frequency variability of renewables are increasingly focusing on large scale climate drivers. These studies reported relationships between climate drivers and wind speeds [17,41,42], solar radiation [43,44] or both variables [16,45]. Establishing these relationships is important for many reasons: they contribute to the exploration of seasonal forecasts [17], they allow to infer about long term trends in the availability of the resources [14], and helps in the understanding of the co-variability and balancing of these resources [45]. The aim of this study is to implement a methodology to define extreme events of solar and wind power production, analyze their impacts on the energy production and complementarity between sources, and to gain insight into their relationships with large-scale climate drivers.

2. Methodology

2.1. Climate data and conversion to wind and solar power

We simulated the hypothetical production of existing and projected wind and solar facilities in Argentina. Wind and solar generation is rather new and is steadily growing in this country; the majority of wind and solar facilities have been deployed within the last three years, and some of them are currently under construction. We considered 46 wind and 21 solar sites, whose locations are shown in Fig. 1. This information was retrieved from the national grid administrator's web page (https://aplic.cammesa.com/geosadi/). The distribution of wind sites span a great portion of the country whereas solar sites are concentrated in the northwestern and Cuyo regions. For each site, we retrieved hourly wind and solar data from the Modern Era Reanalysis for Research and Applications 2 (MERRA2, https://disc.gsfc.nasa.gov/datasets/) [46] at the closest grid point covering the 1980–2019 period, encompassing a total of 350640 data points. For clarification, a meteorological reanalysis is a dataset which assimilates long term historical observational data with simulations from numerical models in a consistent way, and provide relevant variables to compute potential generation from renewables such as wind speeds, surface temperature and solar radiation in a gridded format. Different quality control procedures are performed on the input data at different stages: modeled data from the GEOS-5 model is subjected to a preprocessing quality control at the NASA's Goddard Space Flight Center. MERRA uses a three-dimensional variational data assimilation (3DVAR) analysis algorithm based on the Gridpoint Statistical Interpolation scheme (GSI; [47]); some input data are quality chequed using the GSI Solver. Other conventional datasets (rawinsonde, satellite, precipitation for example) are quality controlled by a sequence of programs prior to being passed to the analysis code [48]. We used wind speeds at 2, 10 and 50 m (variables U2M,V2M,U10M,V10M,U50M,V50M from the M2T1NXSLV data collection); and surface incoming shortwave flux (SWGDN), top-of-atmosphere incoming shortwave flux (SWTDN) and surface skin temperature (TS) from the M2T1NXRAD data collection. Table 1 lists the different variables along with their units. Then, we used conversion models to transform wind speeds and solar radiation into power. For wind power, we applied the Virtual Wind Farm Model (VWFM) model presented in Staffell and Green (2014) and Staffell and Pfenninger (2016) [49,50]. We interpolated wind

Table 1
Meteorological variables retrieved from MERRA2 and their units.

Description	Name	Units
Wind speed	U2M, V2M..	m/s
Surface incoming shortwave flux	SWGDN	W/m^2
Top-of-atmosphere incoming shortwave flux	SWTDN	W/m^2
Surface skin temperature	Ts	° C

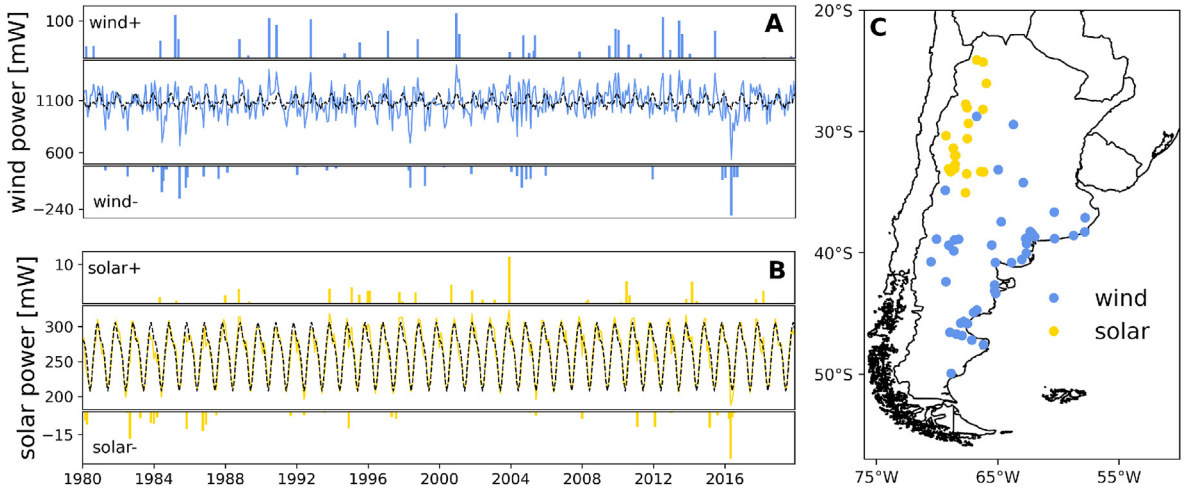

Fig. 1. *a*) Time series of wind power production, average annual cycle of wind power production (black dashed line) *b*) Idem as *a*) but for solar power. Upper and lower panels in *a*) and *b*) depict surplus and deficit events as anomalies in mW *c*) Location of solar (in yellow) and wind (blue) sites.

speeds at each site to 100 mt height using wind speed data at 2, 10 and 50 m height assuming a logarithmic wind profile as in Ref. [50]. We then calculated average wind speeds for each site. Based on those averages, we calculated monthly capacity factors for each site using the power curves of three 3.45 MW commercial wind generators, one for each wind class defined by the International Electrotechnical Commission (IEC) [51]:

- Vestas V126 for mean wind speeds below 8 m/s (class IIB – IIIA)
- Vestas V117 for mean wind speeds between 8 and 9.75 m/s (class IEC IB – IIA)
- Vestas V112 for mean wind speeds above 10 m/s (class IEC IA)

The power curve was then smoothed by applying a gaussian filter in order to emulate the output of multiple turbines within a wind facility. We then convoluted wind speed values with the smoothed power curve.

For solar power, we applied the Global Solar Energy Estimator (GSEE), developed by Pfenninger and Staffel [52]. This method uses the above mentioned SWGDN and SWTDN variables to calculate direct and diffuse radiation via the BRL model [53], which uses several predictors as input such as the clearness index value (the ratio of ground versus top of the atmosphere radiation) and solar altitude. TS is used by the model to adjust the power output through temperature-efficiency curves. Silicon photovoltaic panels are assumed for all sites.

Finally, national wind and solar power production time series were calculated by weighting the capacity factors by the installed capacity at each site and then summing them separately. The comparison between simulated and observed production data is hindered by the low availability of information. Nevertheless, in a previous work [54] we compared our results with data provided by the national grid administrator from 3 wind parks and 1 solar park finding good agreement. We then defined the periods of high and low availability of wind and solar resources (termed *wind+* and *wind-*; and *solar+* and *solar-*). In climatology, extreme events such as droughts can be defined using distribution parameters of the variable being studied (standard deviation for example) [31,55] or thresholds. The latter methodology called the threshold level method [56]. So, an extreme event starts whenever the variable of interest falls below a threshold and finishes when reaches that value again [57]. The main advantage of this method is that no previous knowledge of probability distributions is required; thresholds are often derived from percentiles of the distribution [58]. Moreover, the threshold can be fixed or variable in time [56,59]. It is recommendable to use a variable threshold in the case that the variable of interest has a significant seasonal component [29,60,61]; for example, seasonal streamflow anomalies should not be reported as drought [59]. In our study region, both variables (solar radiation and wind speeds) show significant annual cycles. In addition to the obvious annual cycle of solar radiation, wind speeds present distinct annual cycles over northeastern, central and southern Argentina [14,54]. We defined *wind-* and *solar-* as wind and solar power equal or below for 90% (Q90) of the time; and *wind+* and *solar +* as wind and solar power equal or exceeded for 90% (Q90) of the time. This was performed separately for each month of the year.

2.2. Links with large-scale climatic drivers

We defined complementarity between solar and wind resources as the co-occurrence of events of opposite sign (*wind+*/*solar-* or *wind-*/*solar+*). The significance of these occurrences was tested using a contingency table [62]. We analyzed the influence of five atmospheric and oceanic oscillation indices on the variability of wind and solar resources. The choice of these indices was motivated by previous knowledge about their impacts on the climate variability. Variations in both wind speeds and solar radiation will, in turn, respond to broader scale circulation anomalies; and there is extensive work linking regional climate variations with, for example, sea surface temperatures over different ocean basins [63–65], or extratropical atmospheric variations [66–68]. For these reasons, we chose two indices of the variability of Sea Surface Temperatures (SST) over the Atlantic basin: the Tropical South Atlantic index (TSA), and the Atlantic Multidecadal Oscillation (AMO), one index for the Pacific basin: Multivariate El Niño Index (MEI), one index of the Indian basin: the Dipole Mode Index (DMI), and one index of the extratropical atmospheric circulation: the Antarctic Oscillation (AAO). The AAO is constructed using the leading mode of Empirical Orthogonal Function (EOF) analysis of monthly mean 700 hPa heights [69]. The MEI is the time series of the leading combined EOF of five different variables (sea level pressure (SLP), sea surface temperature (SST), zonal and meridional components of the surface wind, and outgoing longwave radiation (OLR)) over the tropical Pacific basin (30°S-30°N and 100°E–70°W) [70]. The DMI represents the SST gradient between the western equatorial Indian Ocean (50°E–70°E and 10°S-10°N) and the south eastern equatorial Indian Ocean (90°E–110°E and 10°S-0°N) [71]. Finally, AMO and TSA summarize the variability of SSTs over different regions of the Atlantic basin. AMO index is based upon the average anomalies of sea surface temperatures (SST) in the North Atlantic basin over 0°-80°N [72,73]; while the TSA SST anomaly index is an indicator of the surface temperatures over the eastern tropical South Atlantic Ocean (30°W - 10°E, 20°S - 0°) [74].

Several studies reported that the response of local meteorological variables to large scale climate drivers can be seasonally dependent or lagged in time [75]. For these reasons, we performed simultaneous and lagged (up to 8 months) monthly correlations between the previously mentioned climate indices and solar and wind energy production series. The relationships between surplus and deficit events and the phase of the different climate indices was established using contingency tables. In order to discriminate the role of low and high frequency variations in these relationships, we also performed the correlations between high-pass filtered and detrended climate indices and solar and wind energy production series. We implemented a Butterworth high pass filter [76] and subtracted the linear least-squares fit for detrending the time series [77]. Finally, in order to gain insight of the physical mechanisms behind these relationships and their geographical extent, it is necessary to observe different atmospheric and oceanic fields in relation to te variability of solar and wind power. Large-scale climate drivers such as the above mentioned are often originated as atmospheric responses to anomalous sources of heat in the surface of the oceans; and propagate to remote regions as alternating atmospheric pressure anomalies (called wavetrains) which tend to be more discernible at mid and high tropospheric levels [78]. Above the surface of the earth, the conventional vertical coordinate in meteorology is not atmospheric pressure. Instead, it is the geopotential height, which can be defined as the height (in meters above sea level) of a given pressure surface [79]. For a fixed pressure level, regions of low (high) geopotential height are analogs low (high) pressure zones. We composited the fields of anomalies of sea surface temperatures (SSTs), 250 and 500 hpa geopotential heights, Vertically Integrated Flux of Water Vapor (VIFWV), total cloud fraction and wind speeds during the *wind+*, *wind-*, *solar+* and *solar-* events. These composites were computed for all seasons and a number of 12 data points were used for each one. All the above mentioned datasets were retrieved from MERRA2.

3. Results

3.1. Complementarity between wind and solar power

Let us begin describing the variations of wind and solar energy production and the occurrence of extreme events. As expected, solar production shows a strong and prevalent annual cycle whereas wind production shows a much weaker and variable cycle, with a maximum during the warm season (Fig. 2).

This higher variability of wind power can also be seen in Fig. 1, which shows the complete time series of wind and solar power along with the mean annual averages. This figure also depicts the events of deficit and surplus in both wind an solar power as defined in the previous section (*wind-*/*wind+* and *solar+*/*solar-*). As mentioned before, we defined the complementarity as the co-occurrence of events of opposite sign (*wind+*/*solar-* or *wind-*/*solar+*). A contingency table between events (Table 2.) shows a slightly higher tendency than expected of occurrence of events of equal sign (*wind+*/*solar+* and *wind-*/*solar-*), and a lower tendency of occurrence ef events of opposite sign ($\chi_2 = 16.47$, significant at the 99.9% of confidence level). Thus, solar and wind resources show a low complementarity with regard to these events.

3.2. Links with large-scale climatic drivers

We found that the relationships with large scale climate drivers are quite different for wind and solar resources. Fig. 3 shows the correlations between wind and solar time series with time lags. The left column in 3 shows te correlation between the raw time series, while the right column shows the correlation with high-pass filtered and detrended time series. As stated in the methodology section, we filtered low-frequency variations and trends (if present) in order to separate the effect of low and high frequency variability. There is a negative simultaneous correlation between wind power and the Antarctic Oscillation (AAO), mainly during spring and summer. Furthermore, there is a clear tendency towards a higher occurrence of *wind* + events during the negative phase of the AAO and vice-versa (Table 3., $\chi_2 = 16.47$, significant at the 99.9% confidence level). The fact that the correlation pattern is maintained after removing the positive trend in the AAO index shows that this relationship is explained by interannual variations, and not by long-term trends. The signature of the AAO can be distinguished looking at regional atmospheric anomalies associated with *wind+* and *wind-* events (Figs. 4 and 5). *Wind-* (*wind+*) events are associated with high (low) pressure anomalies centered at the Drake Passage/southernmost Patagonia (upper panel in Figs. 4 and 5, centers of low and high pressure anomalies are indicated with letters L and H respectively). The configuration of pressure anomalies observed during spring for both *wind+* and *wind-* events, with three centers of anomalies over the mid latitudes (termed zonal wave number 3) is characteristic of the AAO [80]. During autumn and winter, the positive and negative anomalies over southern Argentina seem to be part of an alternating pattern of pressure anomalies of opposite sign from lower latitudes, but we did not find any significant signal in the SSTs over subtropical nor tropical oceans (not shown), so we think that these signals might be spurious. The associated wind speed anomalies (lower panels in Figs. 4 and 5), nevertheless, do not encompass the totality of wind sites. Positive (*wind+*) and negative (*wind-*) anomalies are centered in Patagonia. But not all sites are located there, which suggests that eventual additions of power outside this region could diminish the impacts of deficit and surplus events.

Table 2
Contingency table showing the frequency of observations of monthly extreme events for wind and solar power, showing low complementarity between them. For each frequency, the percentage above or below the expected value is shown between brackets.

	wind+	*wind−*	total
solar+	5 (+87%)	0 (−100%)	36
solar−	1 (−62.4%)	8 (+200%)	36
total	36	36	

Solar power, on the other hand, seems to be related to ocean-rooted climate variations in both the Pacific and Atlantic basins. Furthermore, the relationships seem to be dominated by different frequencies depending on the ocean basin. Regarding the Atlantic, both the solar time series and the AMO and TSA indices show low frequency variations or trends which result in a tendency towards higher values in recent years. We found a negative simultaneous correlation with the AMO index during april–may, and a positive correlation during spring (Fig. 3, left column). Because of this evident seasonal relationship, we performed the contingency table analysis during the period august–december. It shows a tendency towards a higher frequency of *solar+* during the positive phase of AMO and vice-versa (Table 4, $\chi_2 = 15.12$, significant at the 99.9% confidence level). We found also positive simultaneous correlations with the TSA index throughout the year, but stronger during winter. The contingency table (Table 5, $\chi_2 = 12.05$, significant at the 99.9% confidence level) shows a high frequency of occurrence of *solar+*/TSA + events, and very low frequency (only 1 case) of *solar+*/TSA- events. This positive relationship is not observed for the *solar-* events, and this might be due to the fact that TSA index is skewed towards positive values (not shown). These relationships with the Atlantic AMO and TSA indices are substantially modified after low-frequency variations are removed from the data (right column in Fig. 3). AMO still shows some positive correlations during winter and spring, which are not simultaneous but lagged between 1 and 3 months; while the relationship with the TSA is lost. This means that the relationship between the solar power time series and these

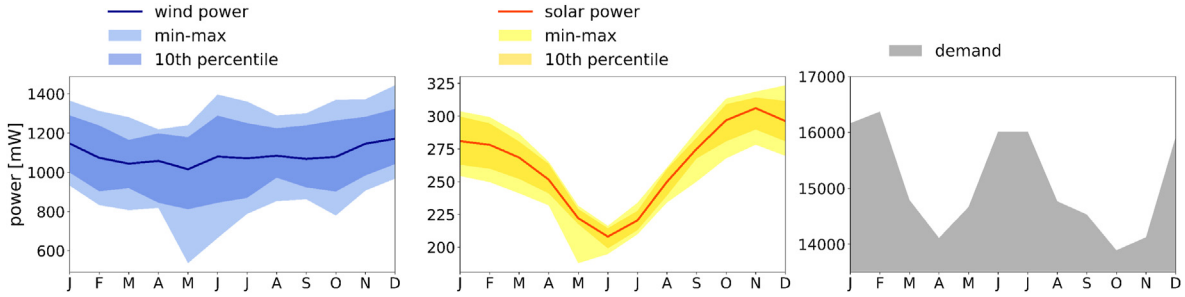

Fig. 2. Average annual variations of wind power (left panel, blue), solar power (middle panel, yellow), and electricity demand (rightr panel, provided by the national grid administrator https://cammesaweb.cammesa.com/).

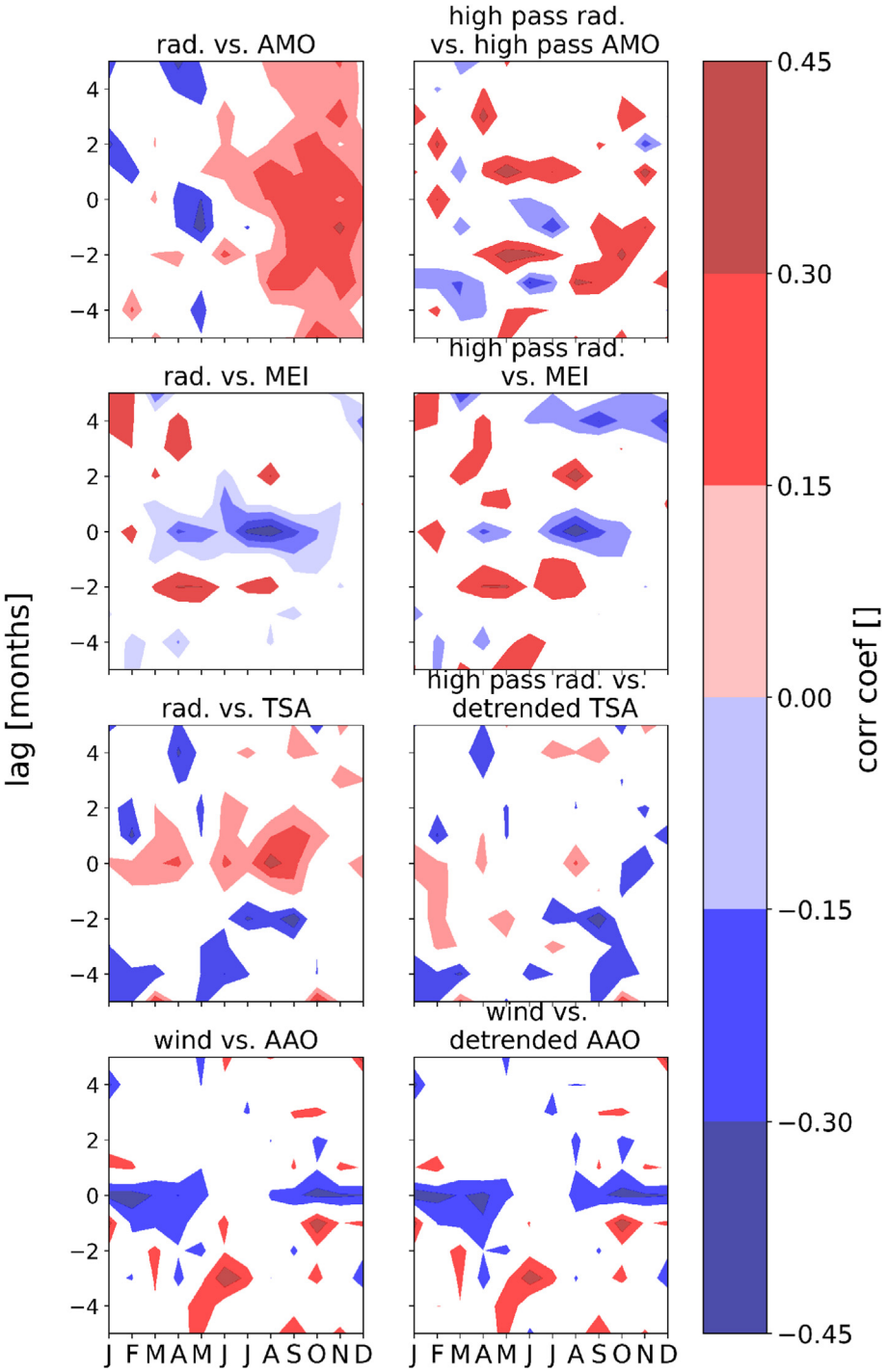

Fig. 3. Correlation map between raw (left column) and filtered or detrended (right column) climate indices and wind and solar time series. Y-axis shows the temporal lags while X-axis indicates the month.

Table 3
Contingency table showing the frequency of observations of wind events and AAO phases. For each frequency, the percentage above or below the expected value is shown between brackets.

	AAO+	AAO-	total
wind+	9 (−59%)	27 (+23%)	36
wind-	27 (+23%)	9 (−59%)	36
total	262	217	

Atlantic variability indices is partly dominated by low-frequency variations. The correlations with El Niño/Southern Oscillation (MEI), on the other hand, are not affected by the removal of low-frequency variations. In this case, we found negative correlations with the MEI index during autumn, winter and spring. This signal being more intense during winter and early spring (Fig. 3). There is a tendency towards a higher occurrence of *solar* + events during the cold phase of El Niño and vice-versa (Table 6, $\chi_2 = 18.27$, significant at the 99.9% confidence level).

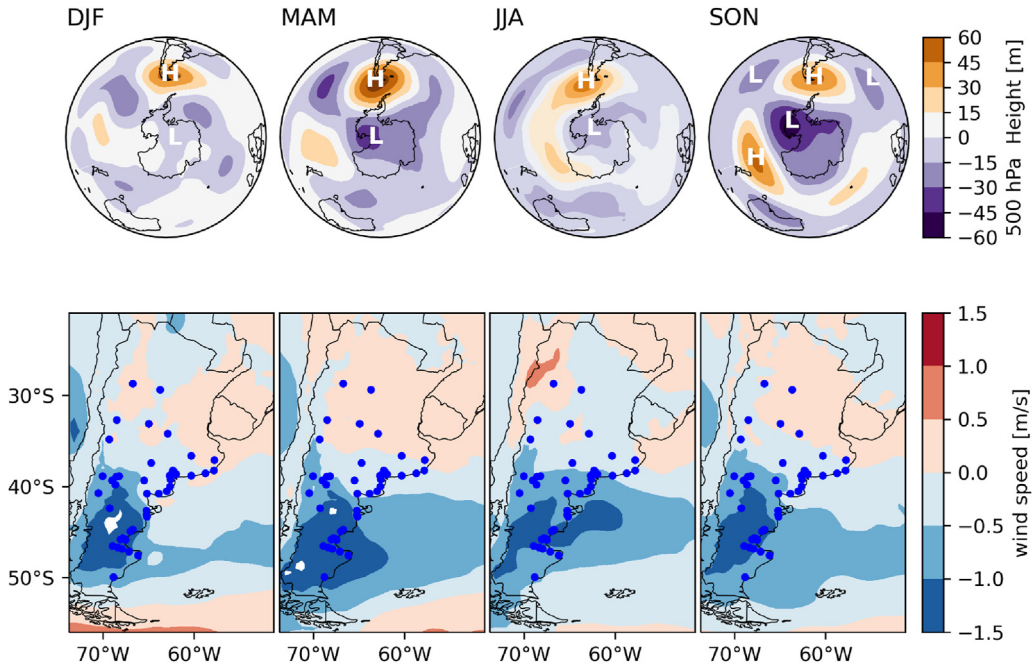

Fig. 4. Seasonal composites of anomalies of 500 hpa geopotential height (upper panel) and wind speeds (lower panel) during the occurrence of *wind-* events. Blue dots indicate the location of wind sites. Centers of low and high pressure anomalies are indicated with letters L and H respectively.

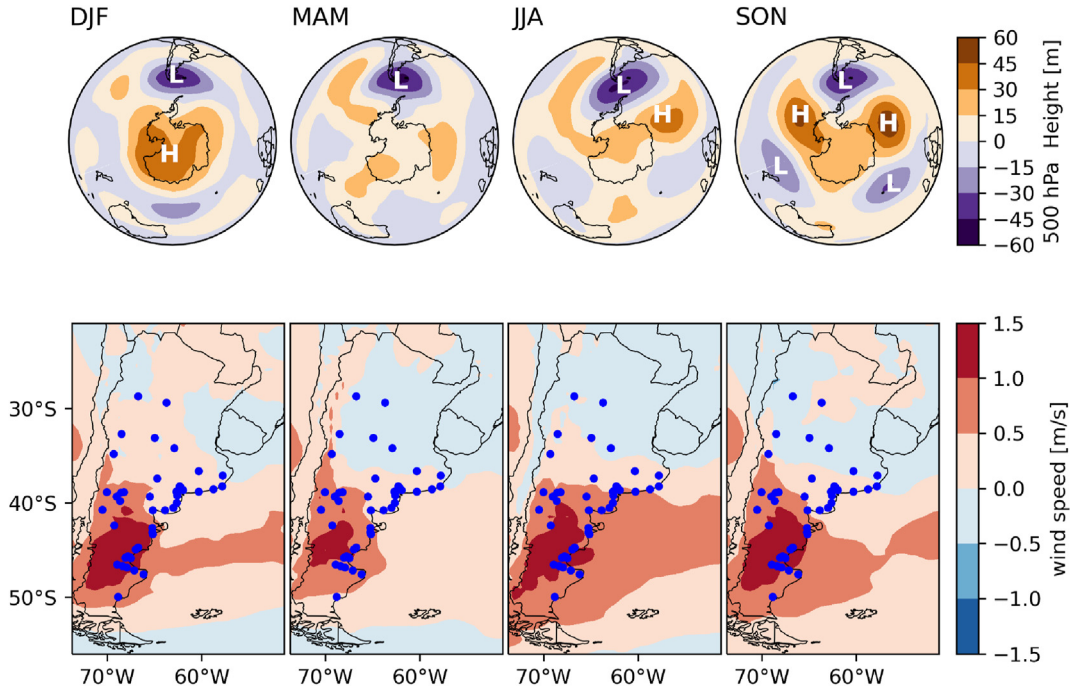

Fig. 5. Seasonal composites of anomalies of 500 hpa geopotential height (upper panel) and wind speeds (lower panel) during the occurrence of *wind* + events. Blue dots indicate the location of wind sites. centers of low and high pressure anomalies are indicated with letters L and H respectively.

Large-scale atmospheric and oceanic fields associated with *solar* events shift throughout the year and evidence the features of the oceanic indices analyzed above (Figs. 6 and 7). *Solar-* events are also associated with positive SSTs anomalies in the tropical Pacific during autumn, winter and spring; which is the signature of the warm phase of El Niño/Southern Oscillation (ENSO) (row b) in Fig. 6). *Solar-* events are associated with different configurations of atmospheric circulation when observing pressure anomalies at higher levels of the troposphere (250 hpa, row a)). During summer and spring *Solar-* events are associated with high pressure anomalies positioned over eastern Patagonia. This patterns do not seem to be part of an organized and discernible pattern of pressure anomalies. During autumn and winter, on the other hand, we found a dipole of negative anomalies centered at approximately 30°and positive anomalies over the Amundsen-Bellinghausen Sea. This configuration is consistent with an alternating pattern of anomalies

Table 4
Contingency table showing the frequency of observations of solar events and AMO phases. For each frequency, the percentage above or below the percentage above or below the expected value is shown between brackets.

	AMO+	AMO-	total
solar+	12 (−33%)	3 (−50%)	15
solar-	4 (−74%)	11 (+83%)	15
total	118	81	

Table 5
Contingency table showing the frequency of observations of solar events and TSA phases. For each frequency, the percentage above or below the expected value is shown between brackets.

	TSA+	TSA-	total
solar+	35 (−28%)	1 (−88%)	36
solar-	23 (−16%)	13 (+61%)	36
total	368	109	

Table 6
Contingency table showing the frequency of observations of solar events and EL Niño/Southern Oscillation phases. For each frequency, the percentage above or below the expected value is shown between brackets.

	MEI+	MEI-	total
solar+	6 (−37%)	18 (+59%)	36
solar-	19 (+100%)	5 (−66%)	36
total	129	153	

that propagates from the tropics (indicated with arrows) and is excited by the warm anomalies in the central tropical Pacific (indicated with an *). This pattern is consistent with the Pacific-South American (PSA) pattern, see Ref. [81]. In any case, these different configurations in the fields of pressure anomalies result in shifts in the circulation at low levels and, hence, the flux of moisture. Rows c) and d) in Fig. 6 show the Vertically Integrated Flux of Water Vapor (VIFWV) and the Cloud Fraction. VIFWV shows northerly anomalies during all seasons, which is consistent with the 250 hpa configurations described above. That is, upper level circulation anomalies seem to be increasing moisture transport from tropical and subtropical South America into the region of interest. During autumn and winter, besides, the presence of cyclonic anomalies above and westward of the Andes range might increase cloudiness at upper levels of the troposphere.

Solar + events are associated with SSTs anomalies over different regions worldwide, mainly over the Pacific and Atlantic basins. Regarding the Pacific basin, *solar* + events are related to the negative phase of ENSO during autumn, winter and spring. That is: cold temperature anomalies along the eastern equatorial Pacific, and warm anomalies over western and subtropical central Pacific (row b) in Fig. 7). During summer, this pattern is slightly different, with warm anomalies over the eastern equatorial Pacific. Positive SSTs anomalies are also observable over the tropical Atlantic during summer, autumn and winter; and over the north Atlantic during summer, winter and spring. The pressure anomalies at the upper levels of the troposphere associated with these events are quite different between summer and the rest of the year (row a) in Fig. 7). Although there are negative anomalies over Patagonia during all seasons, the broader pattern in which these anomalies are embedded differ. During summer, negative geopotential anomalies over Patagonia seem to be part of a west-east oriented pattern which consists of three centers of action. It does not seem to propagate from any particular oceanic region. During the remaining seasons, the negative anomalies over Patagonia seem to be part of a northwest-southeast oriented pattern (indicated with arrows) originating in the subtropics (indicated with an *). This pattern is more zonally oriented during winter and spring, and resembles the atmospheric response of the warm SSTs anomalies over the eastern and tropical Pacific which are described above. Just as with the *solar* + events, the anomalies in the circulation at higher levels of the troposphere result in changes in low level circulation and the regional flux of moisture. The cyclonic gyre is evident with its center east off Argentina's coast in the VIFWV anomalies (row c) of Fig. 7). This gyre results in southerly VIFWV anomalies over the country which counteract the flux of moisture from tropical and subtropical regions of the continent, and reminds the postfrontal meteorological configuration, which is associated with clear skies over central Argentina. Interestingly Garreaud et al. [82] associated a warming in a similar region of the Pacific Ocean (162.58–152.58°W, 33–40°S) with shifts in the southern hemisphere atmospheric circulation over the last two decades, and even with drier conditions over central Chile.

4. Discussion

In this study we analyzed low frequency variations, and their connections with large scale atmospheric and oceanic features, of both wind and solar power over Argentina using reanalysis data. We used MERRA2 solar radiation and wind speed data to estimate wind and solar power time series for a 40 year period. We assessed the occurrence of periods of above and below average wind and solar production (termed *wind+*/*wind-* and *solar+*/*solar-*) using the variable threshold method: we defined these events as the values of both solar and wind power production time series which are below and above 90% (Q90) for each month's distribution separately. We found low complementarity in the occurrence of these events; that is a higher frequency of occurrence of events of the same sign (*solar+* and *wind+*, *solar-* and *wind-*).

The large scale oceanic and atmospheric mechanisms behind both the overall variability of wind and solar time series, and + and - events, are diverse and operate over different timescales. The wind resource is more responsive on the AAO, which is the most important extratropical atmospheric circulation mode of variability in the Southern Hemisphere. This relationship is negative and strongest during spring and summer, which is consistent with previous findings in Ref. [68], and seems to be dominated by high frequency interannual variations and not by long term trends. The AAO index has a positive trend, but the sum of the output of all wind sites has not. This may change if wind sites were individually analyzed: in a previous study ([68]), we found positive and negative trends in wind speeds over different areas throughout Argentina. The stronger signal with the AAO, in comparison with other climate indices such as MEI, might also result from the geographical distribution of wind sites. Most of the sites lie within central Argentina/northern Patagonia, which is the region which shows stronger correlations with the AAO [68].

Variations in the solar resource depend on cloudiness variations, which seem to respond to the variability of SSTs both in the Pacific and the Atlantic basins, according to several studies [63,65,83–85]. Although these studies focused on precipitation (and not on solar radiation), it is likely that variations in precipitation are positively associated with variations in cloudiness. One important caveat when comparing previous studies with our results is that most of these studies focused on a region denominated Southeastern South America (SESA), which includes Paraguay, southern Brazil, eastern Argentina and Uruguay. This region coincides with La Plata basin, which is one of the main watersheds of South America; and the motivation of these studies is that changes in precipitation over this region impact important activities such as agriculture, the production of hydroelectric energy and navigability. Rainfall or

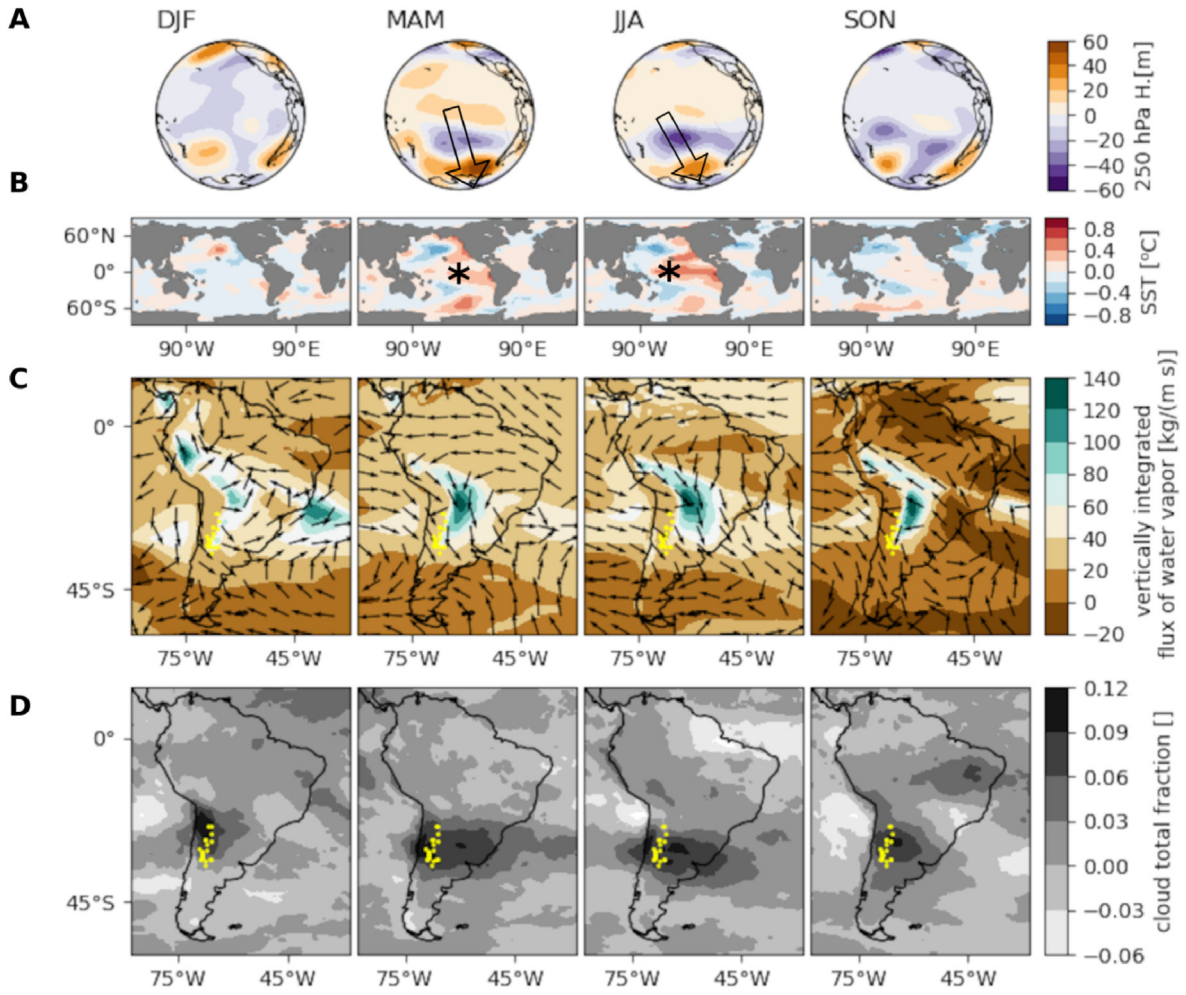

Fig. 6. Seasonal composites of anomalies of 250 hpa geopotential height (row a)), Sea Surface Temperatures (SST row b)), Vertically Integrated Flux of Water Vapor (row c)) and Total Cloud Fraction (row d)) during *solar-* events. Yellow dots indicate the location of solar sites.

cloudiness variations and their connections in our region of interest (Cuyo and northwestern Argentina), on the other hand, had been poorly studied. In fact, there is a scarcity of rainfall measurements in the region.

We found that the relationships between the solar resource and the SSTs operate over different timescales if we consider the Pacific or the Atlantic basins. SSTs in the Pacific seem to influence shorter-term interannual variations, while variations over different regions of the Atlantic (AMO and TSA indices) seem to be associated with longer-term variations and trends. This feature was previously observed by Seager et al. ([84]), who assessed links between precipitation over SESA and SSTs over the tropical oceans.

The examination of composites of anomalies of different oceanic and atmospheric fields enable the formulation of inferences about the possible physical mechanisms behind the relationships we observed. In this sense, we found interesting differences and similarities with previous studies which we will describe hereunder. We found that below average solar power events are associated with northerly anomalies of water vapor fluxes over the region of interest throughout the year, but atmospheric and SST fields show differences between spring-summer and autumn-winter. During spring and summer, the low-level flux of water vapor responds to high pressure anomalies located over Patagonia. During autumn and winter, there seems to be an organized pattern of alternating pressure anomalies of different sign across the Pacific with a north-south orientation, and that it is likely excited by the positive SST anomalies observed over the equatorial Pacific. Above average solar power events, on the other hand, are associated with southerly anomalies of water vapor flux over the region of interest. These southerly anomalies of water vapor at low levels are determined by upper level low pressure anomalies which, in turn, seem to be part of the large-scale atmospheric response to the cold ENSO-like configuration of SST anomalies in the Pacific, at least during winter and spring. Nevertheless, according to previous studies ([63]), both low-level flux of vapor and upper level circulation anomalies could be also related to the positive SST anomalies which are observed over north and tropical Atlantic during summer, winter and spring.

Several authors reported relationships between variability in the SSTs over both the Atlantic and Pacific basins and precipitation over subtropical South America and the flux of vapor from the tropics to the extratropics. As stated before, most studies focused on Southeastern South America, and studied a particular feature which is the South American Low Level Jet (SALLJ), that plays an important role in the transportation of moisture from the Amazon to the subtropics, specifically over the La Plata Basin (LPB). This climatological feature has a northwest-southeast direction over Bolivia, Paraguay and northern Argentina ([85]), and there are no previous studies linking its variability with precipitation nor cloudiness over northwestern Argentina or Cuyo. Regarding the

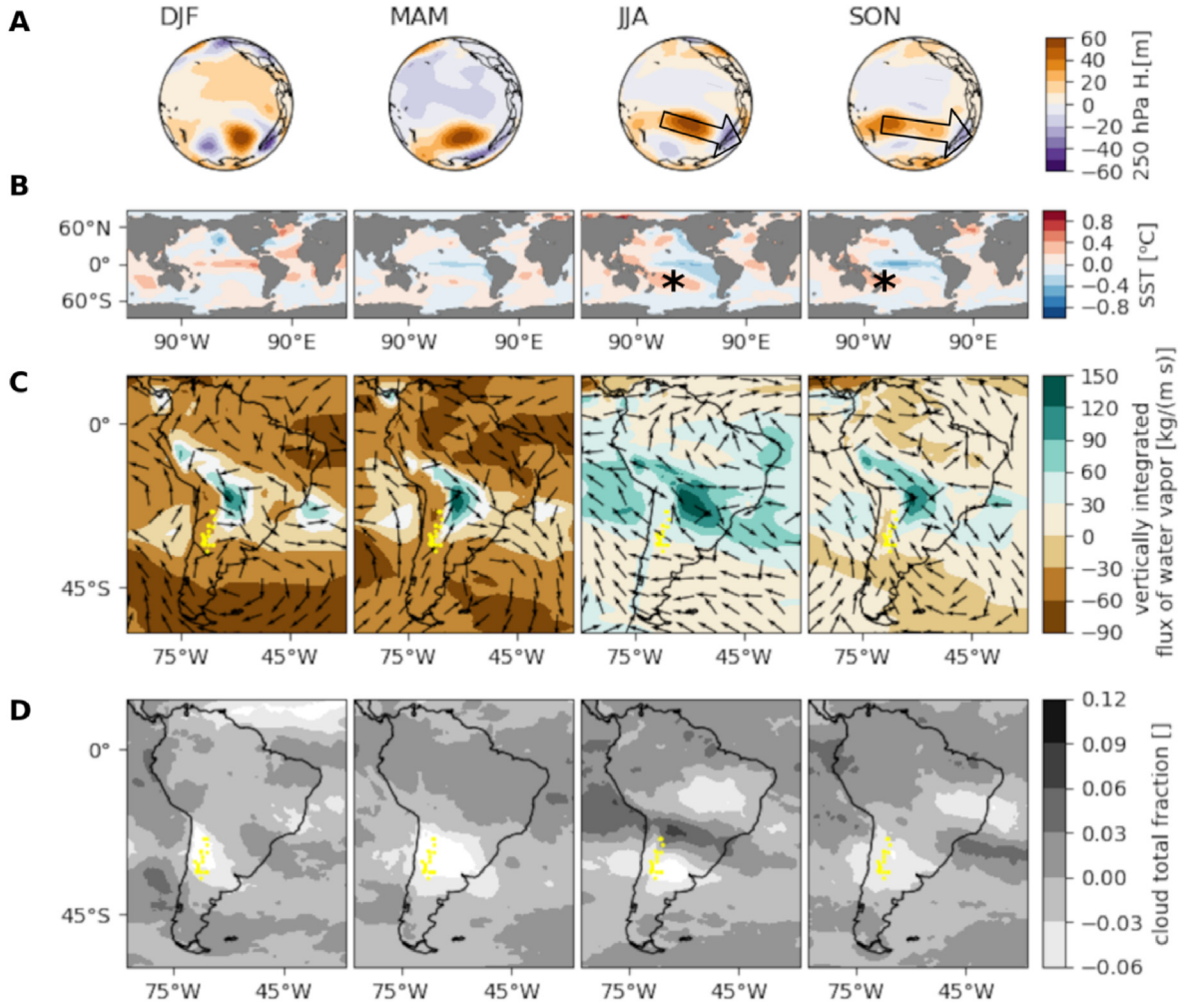

Fig. 7. Seasonal composites of anomalies of 250 hpa geopotential height (row a)), Sea Surface Temperatures (SST row b)), Vertically Integrated Flux of Water Vapor (row c)) and Total Cloud Fraction (row d)) during *solar* + events. Yellow dots indicate the location of solar sites.

relationship between the SALLJ and the Atlantic basin, Jones and Carvalho ([63]) found that the negative phases of AMO are associated with an intensification of the SALLJ and an enhancement of precipitation over southern Brazil, Uruguay and northeastern Argentina. The sign of the relationship is consistent with our findings, but they found it to be stronger during winter while in our case the relationship is stronger during spring and summer. These authors also observed low (high) pressure anomalies at low levels (850 hpa) over Uruguay during the negative (positive) phase of AMO. We did not observe this feature during *solar-* nor *solar* + events. Valdes et al. ([64]) reported negative correlations between AMO and Precipitable Water (PW) over northern Argentina, including our regions of interest. There is not a general consensus about the mechanisms behind the relationship between AMO an the SALLJ. Some authors claim that the positive phase of the AMO is associated with warming in the North Atlantic and cooling in the equatorial Atlantic (TSA region) ([86]). So, during the positive phase AMO, cooling of the western South Atlantic and northward migration of the Inter Tropical Convergence Zone (ITCZ) would lead to decreased intensity of the SALLJ along with a northward displacement of the summer rainfall belt. The opposite would occur during the negative phase of AMO ([87,88]). According to these authors, this signal is strongest during austral summer. This is not entirely consistent with our results since we found a positive correlation between the TSA index and solar power (Fig. 3), meaning that somehow warmer conditions over the tropical Atlantic are related to drier conditions (and hence, clearer skies) over Cuyo and northwestern Argentina. Seager et al. ([84]) propose a different mechanism which happens to be more consistent with our results. First of all, they state that TSA and AMO indices are positively correlated, indicating that the tropical SST anomalies vary in phase with SST anomalies across the North Atlantic Ocean. This can be observed in Fig. 8, which shows the correlations between all indices. AMO and TSA show positive correlations for all seasons. These authors claim that cold tropical Atlantic SST anomalies would lead to wet conditions in SESA. They link long term (decadal) variations in precipitation over SESA with variations in SSTs over the TSA region. The mechanism which explains the relationship between SSTs over the TSA region and precipitation over SESA is, according to these authors, the establishment of a north-south oriented alternating pattern of pressure anomalies (termed Rosssby wave) in response to the tropical heating anomalies; resulting in high pressure anomalies over the southwest South Atlantic Ocean at about 50°S and low pressure anomalies over southern Brazil during cold SST anomalies. Positive (negative) precipitation anomalies would be, in this way, related to dynamically-induced ascent (descent). The sign and the location of these pressure anomalies are consistent with our findings, specially

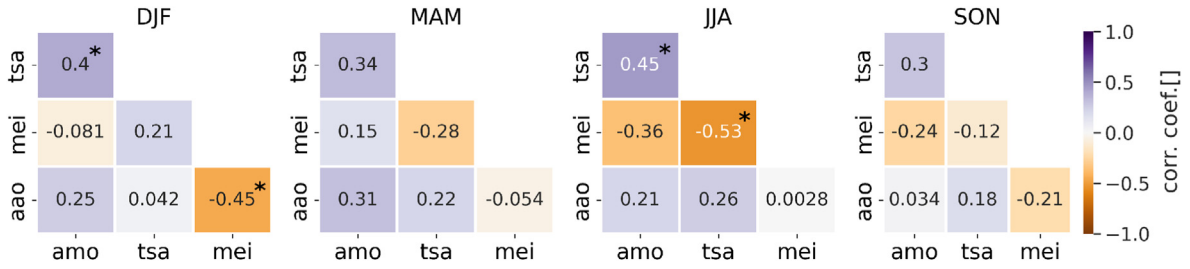

Fig. 8. Seasonal correlations between climate indices. Significant correlation coefficient are indicated with an asterisc *.

for spring and summer during *solar-* events, when the PSA signal is not so clear (see row b) in Fig. 6).

As mentioned before, interannual variability of both the strength and frequency of the SALLJ, which is an important climatological feature that drives moisture from tropical to subtropical south America, is also modulated by the conditions in the Pacific basin. According to Marengo et al. ([87]), Montini et al. ([85]) and Cai et al. ([65]), during warm ENSO events, a pattern of pressure anomalies resembling the Pacific South America (PSA) pattern is associated with an anticyclonic circulation anomaly over eastern Brazil and the subtropical Atlantic and a cyclonic circulation anomaly over southwestern South America and the Pacific which strengthens the subtropical jet stream over SESA, and hence the southward transportation of moisture. This mechanism is strongest during spring. We found similar circulation anomalies over the Pacific during *solar-* events for autumn and winter. But we did not find clear circulation anomalies over the Atlantic. For *solar* + events, however, we found cyclonic anomalies centered at about 40°S matching warm SST anomalies over the equatorial Pacific during summer, and cold SST anomalies during spring (see rows a) and c) in Fig. 7). Anyway, the sign of the upper-tropospheric anomalies over sub subtropical Atlantic with increased precipitation over SESA is opposite to the configuration reported by Seager et al. for cold Atlantic anomalies ([84]). MEI shows negative correlation with both TSA and AMO indices for most of the seasons (see Fig. 8), so these two mechanisms could be reinforcing each other. In this sense, Kayano et al. ([83]) found changing negative and positive interactions between the TSA and ENSO in relation with precipitation variations over northeastern South America during different periods of time. The variations in low-level circulation and vapor flux (and hence, cloudiness) we found are probably a combination of the atmospheric response to both Atlantic and Pacific variations in SST. Part of the differences with previous studies are likely due to the fact that our region of interest is westward of SESA, and the role of the SALLJ on precipitation or cloudiness variations has not been previously studied in this region. Unlike wind sites, which show a wide geographical distribution, solar sites are concentrated in a smaller area (Fig. 1). Future increments in solar capacity will certainly spread across other regions. Especially with the development of rooftop generation. So, the large-scale atmospheric and oceanic controls over the overall solar power production will likely change, and it will become necessary to replicate this study for these other regions.

5. Conclusion

In this study we assessed the occurrence of low frequency extreme events in the availability of wind and solar resources in Argentina; and provided a scheme of the oceanic and atmospheric features related to these events. In a nutshell, the wind resource is associated with a purely atmospheric extratropical feature (the AAO), while the solar resource shows links with SSTs over the Atlantic (TSA and AMO) and the Pacific (MEI) basins. The study of these kind of relationships is of crucial importance for the long term planning and exploitation of renewable energy resources. The frequency and severity of low frequency climatic events is increasingly affecting not only the production of climate-dependent sources of energy, but all kind of economical activities and ecological processes ([89–91]). In our case, the fact that the AAO, AMO and TSA indices show positive trends allow to infer about the future availability of wind and solar resources.

Funding

This work has been entirely supported by the Universidad Nacional de Río Negro.

Author statement

Emilio Bianchi, Tomas Guozden and Roberto Kozulj contributed conception and design of the study. Tomás Guozden and Emilio Bianchi performed the statistical analysis. Emilio Bianchi wrote the first draft of the manuscript. All authors contributed to manuscript revision, read, and approved the submitted version.

Declaration of competing interest

The authors declare that they have no known competing financial interests or personal relationships that could have appeared to influence the work reported in this paper.

References

[1] J. Widén, Correlations between large-scale solar and wind power in a future scenario for Sweden, IEEE Trans. Sustain. Energy 2 (2) (2011) 177–184.
[2] I. Staffell, S. Pfenninger, The increasing impact of weather on electricity supply and demand, Energy.
[3] C.M. Grams, R. Beerli, S. Pfenninger, I. Staffell, H. Wernli, Balancing europe's wind-power output through spatial deployment informed by weather regimes, Nat. Clim. Change 7 (8) (2017) 557.
[4] M. De Felice, A. Alessandri, F. Catalano, Seasonal climate forecasts for medium-term electricity demand forecasting, Appl. Energy 137 (2015) 435–444.
[5] P. Alipour, S. Mukherjee, R. Nateghi, Assessing climate sensitivity of peak electricity load for resilient power systems planning and operation: a study applied to the Texas region, Energy 185 (2019) 1143–1153.
[6] H.C. Bloomfield, D.J. Brayshaw, A.J. Charlton-Perez, Characterizing the winter meteorological drivers of the european electricity system using targeted circulation types, Meteorol. Appl. 27 (1) (2020), e1858.
[7] B. Hamududu, A. Killingtveit, Assessing climate change impacts on global hydropower, Energies 5 (2) (2012) 305–322.
[8] S.W. Turner, M. Hejazi, S.H. Kim, L. Clarke, J. Edmonds, Climate impacts on hydropower and consequences for global electricity supply investment needs, Energy 141 (2017) 2081–2090.
[9] A. K. Raturi, Renewables 2021 Global Status Report.
[10] R. Gross, P. Heptonstall, M. Leach, J. Skea, D. Anderson, T. Green, The UK energy research centre review of the costs and impacts of intermittency, in: Renewable Electricity and the Grid: The Challenge of Variability, 2012, p. 73.
[11] H.C. Bloomfield, D.J. Brayshaw, L.C. Shaffrey, P.J. Coker, H. Thornton, Quantifying the increasing sensitivity of power systems to climate variability, Environ. Res. Lett. 11 (12) (2016), 124025.

[12] I. Van der Hoven, Power spectrum of horizontal wind speed in the frequency range from 0.0007 to 900 cycles per hour, J. Meteorol. 14 (2) (1957) 160–164.
[13] B. François, Influence of winter north-atlantic oscillation on climate-related-energy penetration in europe, Renew. Energy 99 (2016) 602–613.
[14] E. Bianchi, A. Solarte, T. Guozden, Spatiotemporal variability of the wind power resource in Argentina and Uruguay, Wind Energy 22 (8) (2019) 1086–1100.
[15] M. Albadi, E. El-Saadany, Overview of wind power intermittency impacts on power systems, Elec. Power Syst. Res. 80 (6) (2010) 627–632.
[16] D. Pozo-Vazquez, F.J. Santos-Alamillos, V. Lara-Fanego, J.A. Ruiz-Arias, J. Tovar-Pescador, The impact of the nao on the solar and wind energy resources in the mediterranean area, in: Hydrological, Socioeconomic and Ecological Impacts of the North Atlantic Oscillation in the Mediterranean Region, Springer, 2011, pp. 213–231.
[17] R.T. Clark, P.E. Bett, H.E. Thornton, A.A. Scaife, Skilful seasonal predictions for the european energy industry, Environ. Res. Lett. 12 (2) (2017), 024002.
[18] U.B. Gunturu, W. Hallgren, Asynchrony of wind and hydropower resources in Australia, Sci. Rep. 7 (1) (2017) 1–8.
[19] P.J. Coker, H.C. Bloomfield, D.R. Drew, D.J. Brayshaw, Interannual weather variability and the challenges for great britain's electricity market design, Renew. Energy 150 (2020) 509–522.
[20] S. Pryor, R.J. Barthelmie, J. Schoof, Inter-annual variability of wind indices across europe, Wind Energy 9 (1–2) (2006) 27–38. An International Journal for Progress and Applications in Wind Power Conversion Technology.
[21] S. Pryor, R. Barthelmie, Assessing the vulnerability of wind energy to climate change and extreme events, Climatic Change 121 (1) (2013) 79–91.
[22] J. Wohland, N.E. Omrani, N. Keenlyside, D. Witthaut, Significant multidecadal variability in German wind energy generation, Wind Energy Sci. 4 (3) (2019) 515–526.
[23] S. Rose, J. Apt, What can reanalysis data tell us about wind power? Renew. Energy 83 (2015) 963–969.
[24] A. Kies, B.U. Schyska, M. Bilousova, O. El Sayed, J. Jurasz, H. Stoecker, Critical review of renewable generation datasets and their implications for european power system models, Renew. Sustain. Energy Rev. 152 (2021), 111614.
[25] M.J. Hayes, C. Alvord, J. Lowrey, Drought Indices, National Drought Mitigation Center, University of Nebraska, 2002.
[26] L. Dawkins, I. Rusby, Characterising Adverse Weather for the uk Electricity System, Including Addendum for Surplus Generation Events, United Kingdom Meteorological Office.
[27] R. Arabzadeh, M.M. Kholoosi, J. Bazrafshan, Regional hydrological drought monitoring using principal components analysis, J. Irrigat. Drain. Eng. 142 (1) (2016), 04015029.
[28] X. Ye, X. Li, C.-Y. Xu, Q. Zhang, Similarity, difference and correlation of meteorological and hydrological drought indices in a humid climate region—the poyang lake catchment in China, Nord. Hydrol 47 (6) (2016) 1211–1223.
[29] J.A. Rivera, D.C. Araneo, O.C. Penalba, R. Villalba, Regional aspects of streamflow droughts in the andean rivers of patagonia, Argentina. links with large-scale climatic oscillations, Nord. Hydrol 49 (1) (2018) 134–149.
[30] A. Zargar, R. Sadiq, B. Naser, F.I. Khan, A review of drought indices, Environ. Rev. 19 (NA) (2011) 333–349.
[31] S.M. Vicente-Serrano, S. Beguería, J. Lorenzo-Lacruz, J.J. Camarero, J.I. López-Moreno, C. Azorin-Molina, J. Revuelto, E. Morán-Tejeda, A. Sanchez-Lorenzo, Performance of drought indices for ecological, agricultural, and hydrological applications, Earth Interact. 16 (10) (2012) 1–27.
[32] Y. Zhu, J. Chang, S. Huang, Q. Huang, Characteristics of integrated droughts based on a nonparametric standardized drought index in the yellow river basin, China, Nord. Hydrol 47 (2) (2016) 454–467.
[33] J.W. Malloy, D.S. Krahenbuhl, C.E. Bush, R.C. Balling Jr., M.M. Santoro, J.R. White, R.C. Elder, M.B. Pace, R.S. Cerveny, A surface wind extremes ("wind lulls" and "wind blows") climatology for central north America and adjoining oceans (1979–2012), J. Appl. Meteorol. Climatol. 54 (3) (2015) 643–657.
[34] T. Glickman, Z. Walter, Glossary of Meteorology, amer. meteor. soc., 2000, p. 855.
[35] K. Klink, Climatological mean and interannual variance of United States surface wind speed, direction and velocity 1, Int. J. Climatol. 19 (5) (1999) 471–488. A Journal of the Royal Meteorological Society.
[36] A. Wörman, A. Bottacin-Busolin, N. Zmijewski, J. Riml, Spectral decomposition of regulatory thresholds for climate-driven fluctuations in hydro-and wind power availability, Water Resour. Res. 53 (8) (2017) 7296–7315.
[37] R. Quadrelli, J.M. Wallace, A simplified linear framework for interpreting patterns of northern hemisphere wintertime climate variability, J. Clim. 17 (19) (2004) 3728–3744.
[38] H.F. Diaz, El Niño and the Southern Oscillation: Multiscale Variability and Global and Regional Impacts, Cambridge University Press, 2000.
[39] D.W. Thompson, J.M. Wallace, Annular modes in the extratropical circulation. part i: month-to-month variability, J. Clim. 13 (5) (2000) 1000–1016.
[40] H.A. Bridgman, J.E. Oliver, The Global Climate System: Patterns, Processes, and Teleconnections, Cambridge University Press, 2014.
[41] K. Klink, Atmospheric circulation effects on wind speed variability at turbine height, J. Appl. Meteorol. Climatol. 46 (4) (2007) 445–456.
[42] X. Li, S. Zhong, X. Bian, W. Heilman, Climate and climate variability of the wind power resources in the great lakes region of the United States, J. Geophys. Res. Atmos. 115 (D18).
[43] R.J. Davy, A. Troccoli, Interannual variability of solar energy generation in Australia, Sol. Energy 86 (12) (2012) 3554–3560.
[44] K. Mohammadi, N. Goudarzi, Association of direct normal irradiance with el niño southern oscillation and its consequence on concentrated solar power production in the us southwest, Appl. Energy 212 (2018) 1126–1137.
[45] K. Mohammadi, N. Goudarzi, Study of inter-correlations of solar radiation, wind speed and precipitation under the influence of el niño southern oscillation (enso) in California, Renew. Energy 120 (2018) 190–200.
[46] M. Bosilovich, R. Lucchesi, M. Suarez, Merra-2: File Specification.
[47] W.-S. Wu, R.J. Purser, D.F. Parrish, Three-dimensional variational analysis with spatially inhomogeneous covariances, Mon. Weather Rev. 130 (12) (2002) 2905–2916.
[48] M. M. Rienecker, M. Suarez, R. Todling, J. Bacmeister, L. Takacs, H. Liu, W. Gu, M. Sienkiewicz, R. Koster, R. Gelaro, et al., The Geos-5 Data Assimilation System: Documentation of Versions 5.0. 1, 5.1. 0, and 5.2. 0.
[49] I. Staffell, R. Green, How does wind farm performance decline with age? Renew. Energy 66 (2014) 775–786.
[50] I. Staffell, S. Pfenninger, Using bias-corrected reanalysis to simulate current and future wind power output, Energy 114 (2016) 1224–1239.
[51] P. H. Madsen, D. Risø, Introduction to the Iec 61400-1 Standard, Risø National Laboratory, Technical University of Denmark.
[52] S. Pfenninger, I. Staffell, Long-term patterns of european pv output using 30 years of validated hourly reanalysis and satellite data, Energy 114 (2016) 1251–1265.
[53] B. Ridley, J. Boland, P. Lauret, Modelling of diffuse solar fraction with multiple predictors, Renew. Energy 35 (2) (2010) 478–483.
[54] T. Guozden, J.P. Carbajal, E. Bianchi, A. Solarte, Optimized balance between electricity load and wind-solar energy production, Front. Energy Res. 8 (2020) 16.
[55] S. Shukla, A. W. Wood, Use of a standardized runoff index for characterizing hydrologic drought, Geophys. Res. Lett. 35 (2).
[56] J.H. Sung, E.-S. Chung, Proposal and application of water deficit-duration-frequency curve using threshold level method, J. Korea Water Resour. Assoc. 47 (11) (2014) 997–1005.
[57] K. Stahl, Hydrological Drought: A Study across Europe, Ph.D. Thesis, Institut für Hydrologie der Universität, 2001.
[58] A.F. Van Loon, Hydrological drought explained, Wiley Interdiscipl. Rev.: Water 2 (4) (2015) 359–392.
[59] A. Van Loon, G. Laaha, Hydrological drought severity explained by climate and catchment characteristics, J. Hydrol 526 (2015) 3–14.
[60] S. Parry, J. Hannaford, B. Lloyd-Hughes, C. Prudhomme, Multi-year droughts in europe: analysis of development and causes, Hydrol. Res. 43 (5) (2012) 689–706.
[61] M. Van Huijgevoort, P. Hazenberg, H. Van Lanen, R. Teuling, D. Clark, S. Folwell, S. Gosling, N. Hanasaki, J. Heinke, S. Koirala, et al., Global multi-model analysis of hydrological drought in the second part of the 20th century (1963–2000), J. Hydrometeorol. 14 (2013) 1535–1552.
[62] H. A. Panofsky, G. W. Brier, W. H. Best, Some Application of Statistics to Meteorology.
[63] C. Jones, L.M. Carvalho, The influence of the atlantic multidecadal oscillation on the eastern andes low-level jet and precipitation in south America, NPJ Clim. Atmos. Sci. 1 (1) (2018) 1–7.
[64] R. Valdés-Pineda, J. Cañón, J.B. Valdés, Multi-decadal 40-to 60-year cycles of precipitation variability in Chile (south America) and their relationship to the amo and pdo signals, J. Hydrol. 556 (2018) 1153–1170.
[65] W. Cai, M.J. McPhaden, A.M. Grimm, R.R. Rodrigues, A.S. Taschetto, R.D. Garreaud, B. Dewitte, G. Poveda, Y.-G. Ham, A. Santoso, et al., Climate impacts of the el niño–southern oscillation on south America, Nat. Rev. Earth Environ. 1 (4) (2020) 215–231.
[66] R.D. Garreaud, M. Vuille, R. Compagnucci, J. Marengo, Present-day south american climate, Palaeogeogr. Palaeoclimatol. Palaeoecol. 281 (3–4) (2009) 180–195.
[67] G. Silvestri, C. Vera, Nonstationary impacts of the southern annular mode on southern hemisphere climate, J. Clim. 22 (22) (2009) 6142–6148.
[68] E. Bianchi, A. Solarte, T.M. Guozden, Large scale climate drivers for wind resource in southern south America, Renew. Energy 114 (2017) 708–715.
[69] K.C. Mo, Relationships between low-frequency variability in the southern hemisphere and sea surface temperature anomalies, J. Clim. 13 (20) (2000) 3599–3610.
[70] K. Wolter, M.S. Timlin, El niño/southern oscillation behaviour since 1871 as diagnosed in an extended multivariate enso index (mei. ext), Int. J. Climatol. 31 (7) (2011) 1074–1087.
[71] N. Saji, B. Goswami, P. Vinayachandran, T. Yamagata, A dipole mode in the tropical indian ocean, Nature 401 (6751) (1999) 360–363.
[72] D.B. Enfield, A.M. Mestas-Nuñez, P.J. Trimble, The atlantic multidecadal oscillation and its relation to rainfall and river flows in the continental us, Geophys. Res. Lett. 28 (10) (2001) 2077–2080.
[73] K. Trenberth, R. Zhang, N.C. for Atmospheric Research Staff, The Climate Data Guide: Atlantic Multi-Decadal Oscillation (Amo), 2019.
[74] J. Servain, Simple climatic indices for the tropical atlantic ocean and some applications, J. Geophys. Res.: Oceans 96 (C8) (1991) 15137–15146.
[75] C.F. Ropelewski, M.S. Halpert, Global and regional scale precipitation patterns associated with the el niño/southern oscillation, Mon. Weather Rev. 115 (8) (1987) 1606–1626.
[76] I.W. Selesnick, C.S. Burrus, Generalized digital butterworth filter design, IEEE Trans. Signal Process. 46 (6) (1998) 1688–1694.

[77] P. Talkner, R.O. Weber, Power spectrum and detrended fluctuation analysis: application to daily temperatures, Phys. Rev. 62 (1) (2000) 150.
[78] I.N. James, Introduction to Circulating Atmospheres, Cambridge University Press, 1995.
[79] J.R. Holton, An introduction to dynamic meteorology, Am. J. Phys. 41 (5) (1973) 752–754.
[80] D. Gong, S. Wang, Antarctic oscillation: concept and applications, Chin. Sci. Bull. 43 (9) (1998) 734–738.
[81] J. Turner, The el nino–southern oscillation and Antarctica, Int. J. Climatol. 24 (1) (2004) 1–31. A Journal of the Royal Meteorological Society.
[82] R.D. Garreaud, K. Clem, J.V. Veloso, The south pacific pressure trend dipole and the southern blob, J. Clim. 34 (18) (2021) 7661–7676.
[83] M.T. Kayano, C.P. de Oliveira, R.V. Andreoli, Interannual relations between south american rainfall and tropical sea surface temperature anomalies before and after 1976, Int. J. Climatol. 29 (10) (2009) 1439–1448. A Journal of the Royal Meteorological Society.
[84] R. Seager, N. Naik, W. Baethgen, A. Robertson, Y. Kushnir, J. Nakamura, S. Jurburg, Tropical oceanic causes of interannual to multidecadal precipitation variability in southeast south America over the past century, J. Clim. 23 (20) (2010) 5517–5539.
[85] T.L. Montini, C. Jones, L.M. Carvalho, The south american low-level jet: a new climatology, variability, and changes, J. Geophys. Res. Atmos. 124 (3) (2019) 1200–1218.
[86] M. Martín-Rey, I. Polo, B. Rodríguez-Fonseca, T. Losada, A. Lazar, Is there evidence of changes in tropical atlantic variability modes under amo phases in the observational record? J. Clim. 31 (2) (2018) 515–536.
[87] J.A. Marengo, W.R. Soares, C. Saulo, M. Nicolini, Climatology of the low-level jet east of the andes as derived from the ncep–ncar reanalyses: characteristics and temporal variability, J. Clim. 17 (12) (2004) 2261–2280.
[88] C. M. Chiessi, S. Mulitza, J. Pätzold, G. Wefer, J. A. Marengo, Possible impact of the atlantic multidecadal oscillation on the south american summer monsoon, Geophys. Res. Lett. 36 (21).
[89] R. Garreaud, Record-breaking climate anomalies lead to severe drought and environmental disruption in western patagonia in 2016, Clim. Res. 74 (3) (2018) 217–229.
[90] C.S. Vera, M. Osman, Activity of the southern annular mode during 2015–2016 el niño event and its impact on southern hemisphere climate anomalies, Int. J. Climatol. 38 (2018) e1288–e1295.
[91] R.D. Garreaud, J.P. Boisier, R. Rondanelli, A. Montecinos, H.H. Sepúlveda, D. Veloso-Aguila, The central Chile mega drought (2010–2018): a climate dynamics perspective, Int. J. Climatol. 40 (1) (2020) 421–439.